Shahrood University of Technology

Journal of Mining and Environment (JME)

Journal homepage: www.jme.shahroodut.ac.ir

Iranian Society of Mining Engineering (IRSME)

# Alteration Mineral Mapping Using the Hyperion Hyperspectral Imagery in Astarghan Area, Northwest Iran

Rashed Pourmirzaee[1*], and Hadi Jamshid Moghadam[2]

*1. Department of Mining Engineering, Urmia University of Technology, Urmia, Iran,*
*2. Faculty of Mining Engineering, Sahand University of Technology, Tabriz, Iran*

***Article Info***

*Received 9 May 2024*
*Received in Revised form 7 June 2024*
*Accepted 28 June 2024*
*Published online 28 June 2024*

*DOI: 10.22044/jme.2024.14503.2723*

***Keywords***

*Hyperion data*
*Match filtering*
*Moving threshold*
*Mineral mapping*

***Abstract***

In recent years, hyperspectral data have been widely used in earth sciences because these data provide accurate spectral information of the earth's surface. This research aims to apply match filtering (MF) on Hyperion hyperspectral imagery for mapping alteration mineral in the Astarghan area, NW Iran. Astarghan is located in the northwest of Iran where deposits of low-sulfide gold-bearing ore rocks occur as veins and stockworks. Therefore, at first, the Astarghan Hyperion scene was topographically and atmospherically corrected. Then, the data quality was surveyed to recognize bad bands and improve the accuracy of the subsequent processing steps. In MF analysis, it is a challenge to separate MF abundance images to target and background pixels. Therefore, to cope with this challenge, a moving threshold technique is proposed. The results indicated three indicative minerals including kaolinite, opal and jarosite. Then, the results were statistically verified by virtual verification and geological data. The verification was performed virtually using United States Geological Survey (USGS) spectral library data, which showed an agreement of 78.06%. Moreover, a comparison of the MF analysis results showed a good agreement with field investigations and overlaying with a detailed geological map of the study area. Finally, in this study the X-ray diffraction (XRD) of three indicative mineral samples was used to check the efficiency of the applied method.

## 1. Introduction

In recent years, remote sensing has become one of the most interesting fields among earth science subjects due to its wide range of applications and capabilities for different studies. One of the most important geological applications of remote sensing is the mapping of key alteration minerals that is vital for ore exploration. These data have been widely used in mineral prospecting and exploration of mineral deposits [1-3].

In a classification, remote sensing optical images are divided into hyperspectral and multispectral data. Multispectral data are a type of remote sensing data that capture reflectance across multiple bands of the electromagnetic spectrum. It typically has 5 to 30 bands that collect data in visible, near-infrared, shortwave infrared, and thermal infrared bands. However, Hyperspectral data capture reflectance across a continuous range of wavelengths. These data usually have hundreds or more bands and provide a more acceptable level of spectral resolution [4,5].

Therefore, hyperspectral remote sensing data analysis allows one to recognize individual materials such as minerals regarding their reflectance characteristics [4, 6, 7]. Hyperion space-borne hyperspectral data became available for more studies of earth surface structures and ore exploration in November 2000.

Several studies have used Hyperion data for geological and mineralogical surveys [8]. A detailed investigation of Hyperion capabilities in mineralogical mapping was implemented by Kruse [6] through comparing airborne visible/infrared imaging spectrometer (AVIRIS) and Hyperion data for mineral mapping across Nevada and California, USA. The results confirmed that the Hyperion

Corresponding author: Poormirzaee@gmail.com (R. Pourmirzaee)

short-wave infrared (SWIR) data are capable of producing useful geologic information.

Cudahy et al. [9] investigated the capability of visible/near-infrared (VNIR) and SWIR bands of Hyperion data for mineral potential mapping at Mountain Fitton, South Australia. There was a good correspondence between mineral distribution (particularly in SWIR data), geology, and alteration maps. Gersman et al. [4] successfully detected hydrothermally altered rocks and mapped different lithological units at the Northern Danakil Depression in Eritrea.

Pour and Hashim [10] used Hyperion and ALI images to map key minerals of hydrothermal alteration halos related to porphyry copper ore deposits in SE Iran. For this purpose, they began with ALI data to map lithological units on a regional scale and then analyzed SWIR Hyperion data to distinguish propylitic, argillic, and phyllic alteration zones.

Oskouei and Babakan [8] analyzed the Hyperion data of the Lahroud region in northwestern Iran to map alteration minerals. As a result, the low SNR of the Hyperion sensor tended to impose some difficulties, but considering the associated costs and time required for field studies, the results of Hyperion data analysis served as a valuable tool for prospecting and reconnaissance studies.

Ekanayake et al. [11], using image processing techniques on Hyperion data, successfully mapped an ilmenite deposit in Pulmudai, Sri Lanka. Vignesh and Kiran [12] carried out a comparative analysis of mineral mapping for Hyperion and Landsat-8 OLI data. They concluded that due to large reflectance bands in short bandwidth intervals, Hyperion shows better results than Landsat-8 OLI.

In addition, other applications of Hyperion data in mineral exploration are shown in [13, 14, 15, 16, 17].

In this study, the capabilities of Hyperion data in terms of mapping alteration minerals in the Astarghan area were investigated. For this aim, after preprocessing steps, the Hyperion data were unmixed through the standard approach developed for analytical imaging and geophysics (AIG). Then, the distribution of extracted endmembers (i.e. alteration minerals) was obtained using the MF, a spectral matching algorithm [18]. In the current study, to map alteration minerals accurately, the MF together with the moving threshold were applied on Hyperion data. Moving threshold is a suitable tool for classifying the MF abundance maps of the endmembers to target and background pixels [19]. This method was tested on HyMap airborne data that have a high spectral and spatial resolution and the results were acceptable, but have not been tested so far on space-born data such as Hyperion. In the present study, three indicative minerals were distinguished across the study area: kaolinite, opal, and jarosite. The method's accuracy was assessed by a virtual verification through of the region. The evaluations showed that the applied method for Hyperion image analysis was an efficient tool to map the alteration minerals. This consistency was confirmed by the XRD results of three samples collected from three indicative mineral units distinguished from the study area.

### 1.2. Geological setting

Astarghan area is approximately located 50 km north of Tabriz, northwest Iran (Figure1). The study area is in the Gharadagh-Arasbaran metallogenic zone [20, 21]. The most important lithological units in the area are a hypabyssal porphyritic granodioritic intrusive stock (Oligo-Miocene) and a flysch-type sedimentary sequence consisting of limestone, limy sandstone, and marl (Paleocene-Eocene) [22]. The intrusion of this stock into the sedimentary rocks has altered them to a series of metasomatic and metamorphic rocks along the contact zone. Potassic, propylitic, argillic, and phyllic alteration zones are developed surrounding the fractured and brecciated zones in the study area. However, the argillic alteration zone represents the dominant alteration zone in the Astarghan area. Instances of Au, Cu, and Sb mineralization have occurred at different parts of the area as porphyry, stockwork, and vein-type mineralization. Ore rock in the Astarghan area is of low-sulfide gold-bearing type and appears as veins, vein zones, and stockworks with quartz and subordinate amounts of sulfide and other metallic minerals [21]. Astarghan's epithermal gold deposit is the main mine across the region.

Furthermore, the flysch sequence was thermally metamorphosed following the emplacement of the Astarghan stock, and resulted in the development of skarn patches, hornfels and marble. The major skarn patches crop out mainly at Kaghdara (Zone A). Volcanic rocks comprised of andesitic and trachytic lavas and stuffs have an intimate relationship with intrusive rocks and probably represent their igneous equivalents. They are mainly seen at topographic heights of the area (e.g., at Nowrozkala) and show the impacts of tectonic activities in the form of numerous joints and

fractures. Two dike generations (1–40 m thick) cut the stock, metasomatites, and sedimentary rocks, which have been characterized by their composition, mineral assemblage, and general trend. Finally, Quaternary alluvial deposits, alluviums and terraces are the youngest units in the study area [21]. The detailed 1:20000 geological map of the Astarghan region is illustrated in Figure 1.

## 2. Data analysis

### 2.1. The Hyperion Scene

The Hyperion instrument provides hyperspectral data for geological purposes and mineral exploration. Hyperion is composed of VNIR and SWIR spectrometers. Nevertheless, Hyperion's poor calibration has caused several deficiencies (e.g. smile effect and vertical strips) in the VNIR/SWIR regions [23]. Correcting these effects will help to accurately identify minerals and other targets. This study processes about 90 km$^2$ of Hyperion scene obtained on 30 November 2004.

### 2.2. Preprocessing

The preprocessing of data is a significant step to get reliable results from the remotely sensed images. All errors and unwanted occurrences that may arise during various steps of data collection are corrected in the preprocessing phase. Being in level 1R (L1R), the Astarghan Hyperion scene has already undergone some preprocessing steps by USGS such as echo removal and smear correction [24].

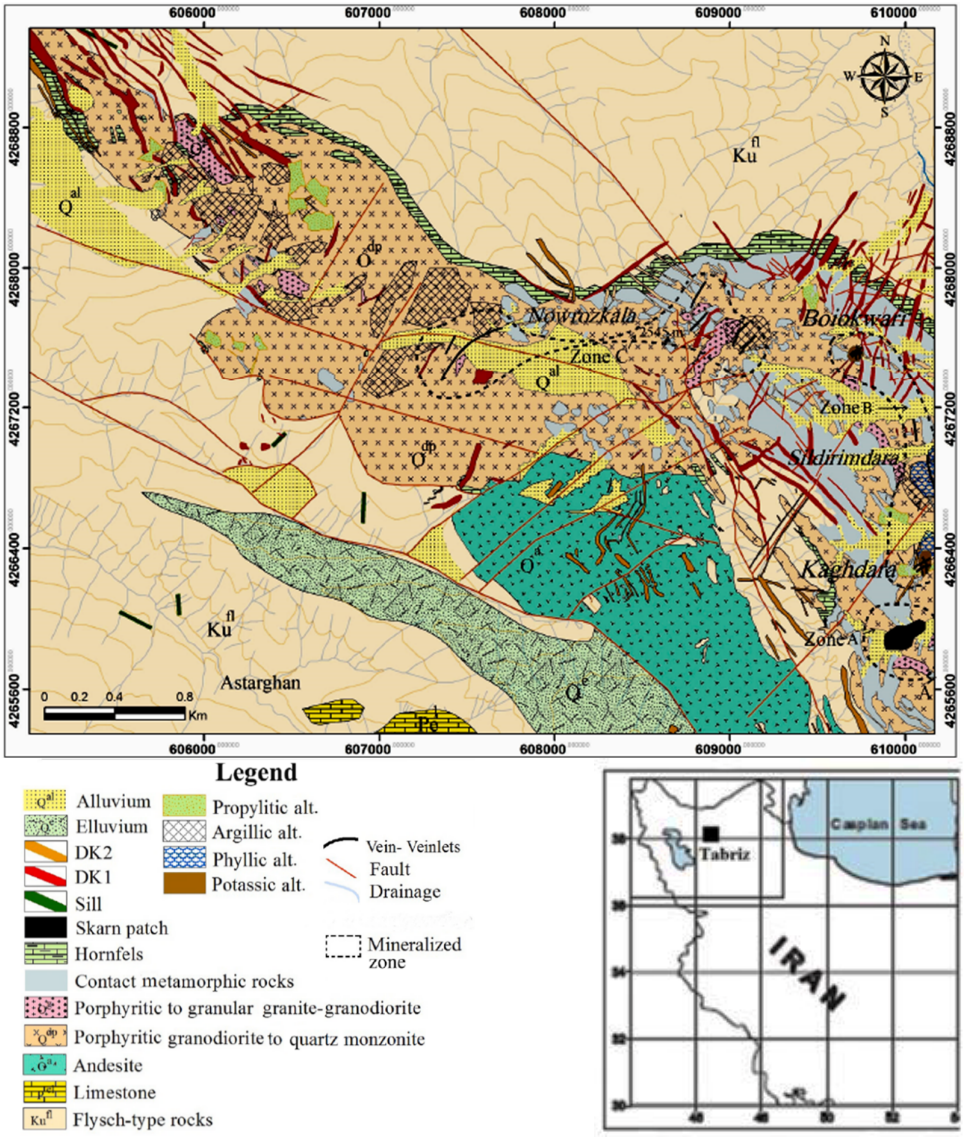


**Figure 1. Location map of the Astarghan region and surrounding geological formations [21].**

### 2.2.1. Destriping

Inaccurate co-calibration of the individual detectors on the focal plane array (FPA) causes severe stripping on Hyperion images that is the so-called stripping effect [25]. The intensity of striping in a band depends on its wavelength, and column number corresponding to the position of the detector on the two-dimensional FPA [26]. The striping effect could reduce classification accuracy of minerals in the study area. Scheffler and Karrasch [26] investigated the most popular available striping removal techniques in detail. Three approaches have been recognized as suitable techniques for image striping correction from different methods proposed for striping removal: i) wavelet Fourier adaptive filtering [27], ii) ENVI general purpose utilities – destripe [28], and iii) ENVI spectral processing exploitation and analysis resource (SPEAR) tools. In this work, ENVI SPEAR tools-vertical destripe removal was applied to remove Hyperion stripes.

### 2.2.2. Smile effect

In order to accurately analyze spectral Hyperion data, especially in the case of mineral mapping, the smile effect needs to be corrected [29]. The smile effect is an interior effect of a sensor that mainly appears in hyperspectral data especially Hyperion [26]. Different methods, i.e., moving linear fitting and interpolation, column mean adjusted in radiance space and column mean adjusted in MNF space [30] have been developed to correct the smile effect. In the current study, the smile effect was removed using column mean adjusted in radiance space through the "cross-track illumination corrections" module, provided within the ENVI software [28].

### 2.2.3. Atmospheric and topographic corrections

The atmospheric effect causes errors in remotely sensed data by reducing the results' accuracy. To compensate for this effect, an atmospheric correction is necessary for converting radiance to reflectance data. Several algorithms such as the atmospheric removal (ATREM), the fast line-of-sight atmospheric analysis of spectral hypercubes (FLAASH), atmospheric correction (ATCOR), and atmospheric correction now (ACORN) [6] have been introduced for atmospheric correction. This study implements the FLAASH algorithm to Hyperion data. The FLAASH calculates the apparent reflectance through the MODTRAN (moderate resolution atmospheric transmission) algorithm [31]. Another radiometric effect on remote sensing imagery is the distortions due to the topography of the earth's surface (Figure2). Topographic correction or elimination of terrain-dependent illumination in rugged terrains is also crucial. The main topographic correction techniques include cosine, Minnaert, and statistical-empirical [32]. Due to its straightforward and reliable functionality, this study used the cosine correction method. Accordingly, the cosine algorithm was programmed in interactive data language (IDL) and utilized for topographic correction of the Hyperion dataset.

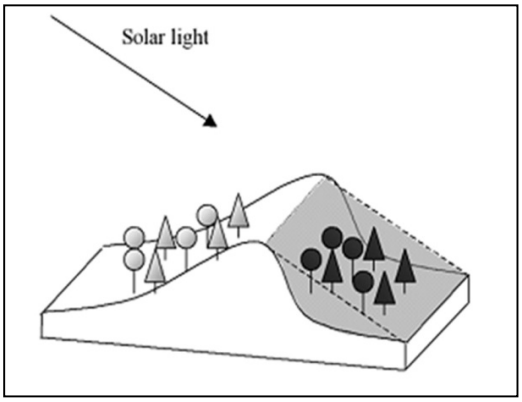


**Figure 2. Topographic effects on reflectance [33].**

Once atmospheric and topographic effects were corrected, the Hyperion data were qualitatively assessed. The presence of noisy bands in data causes errors in the output mineralogical distribution map. Among various approaches used in bands' quality evaluation of hyperspectral data, the signal-to-noise ratio (SNR) determination is a popular one. Most of these approaches are conducted by comparing the ratio of mean spectral response to the corresponding standard deviation. Therefore, the mean-to-standard deviation ratio was used as the approximation of the SNR in this study. The bands with significantly lower SNR values were marked as noisy or bad bands. Moreover, the un-calibrated bands (1-7, 58-76, and 225-242) and spectrally overlapping bands (57, 77) were added to the bad bands list. Then, bad bands were deleted from the dataset. Finally, only 139 good bands (out of 242 total bands) were selected to perform the unmixing task.

The order of steps for the preprocessing of remote sensing data plays a significant role. For example, applying an atmospheric or topographic correction before removing sensor internal errors or incorrect detector calibration may end up with wrong results [34]. Thus, to achieve trustworthy

results, the Hyperion dataset of the study area was corrected following the sequence shown in Figure 3.

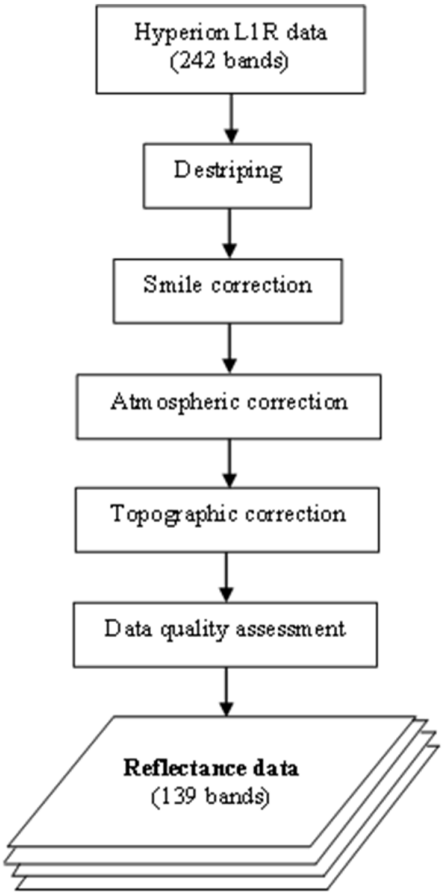


**Figure3. Preprocessing workflow for Hyperion data of study area.**

## 3. Results

### 3.1. Processing

Spectral unmixing is a procedure for the separation of a mixed pixel of remote sensing image to its main constituents. Generally, two models are used to unmix remote sensing images: 1) linear mixture model (LMM) and 2) non-linear mixing model (NLMM). In the LMM, a mixed pixel spectrum is considered to be a linear mixture of the endmembers weighted by their fractions inside the pixel. Thus, if there are M endmembers, the LMM could be demonstrated by equation (1).

$$x = \sum_{t=1}^{q} a_t s_t + w = Sa + N \quad (1)$$

Where $x$ is the pixel spectrum ($L \times 1$ vector) , $S$ is the $L \times q$ endmembers matrix ($L$ and $q$ are the number of bands and endmembers respectively), $s_t$, $t = 1, \dots, q$, $a$ is the $q \times 1$ aboundance vector whose elements are $a_t$, $t = 1, \dots, M$, and $N$ is the $L \times 1$ noise spectrum [35, 36].

On the other hand, if pixels of remote sensing images comprise of non-uniform materials or different compositions, reflections may diffuse into one another. In this case, scattering causes systematic nonlinear mixing of different components of the pixel. Because of its efficiency and simplicity in many case studies, LMM is the most common model in the development of unmixing algorithms. The main obstacle along the path to implement the NLMM is the large number of parameters contributing to the solution, so that complicated equations are needed to apply this method [36, 37].

#### 3.1.1 Endmember extraction

To spectrally analyze remote sensing data, one should select an endmember through either of the following two approaches: 1) selecting the endmembers from the USGS spectral library, or 2) extracting the endmembers from image analysis. The extracted endmember using the latter approach is more reliable as it is obtained in the same conditions as those of the data being processed [19]. Therefore, for mineral mapping and alteration studies, it is better to select endmembers' spectra from the image rather than spectral libraries. In the current study, the endmembers were extracted from Hyperion imagery and to extract mineralogical information, standardized AIG method was used [6]. The AIG is a stepwise algorithm provided in the ENVI software package [28] that can be implemented for processing of remotely sensed data (Figure4). To effectively detect endmembers of hyperspectral data, it is essential to decrease dimensionality and undertake noise separation. Minimum noise fraction (MNF) [38, 39] is a useful technique for denoising Hyperion hyperspectral data. Accordingly, lower-order MNF bands are removed from the next processing steps. Then, pixel purity index (PPI) analysis [36, 38] is performed to find extreme pixels from higher-order MNF bands that are assumed as the purest endmembers.

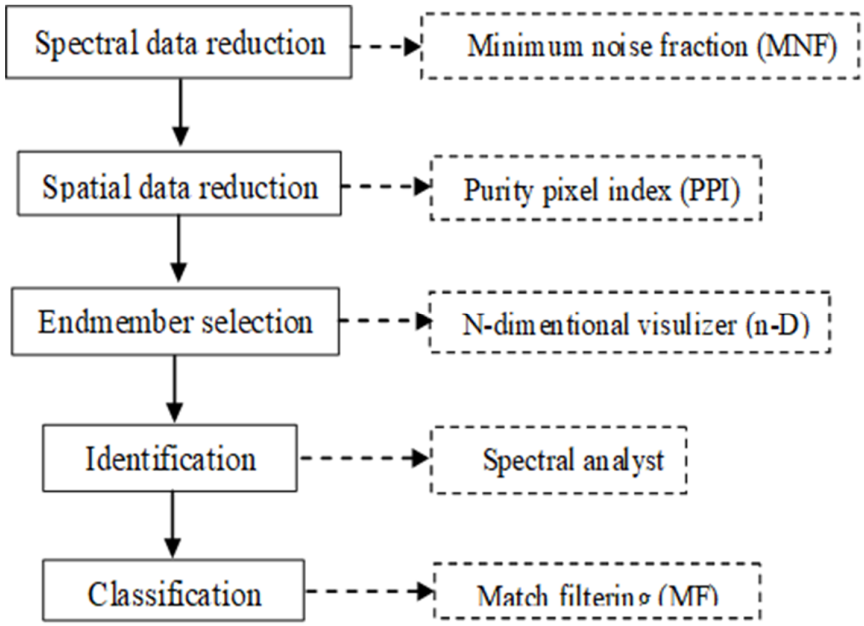


**Figure 4. a block diagram of standardized AIG method for Hyperion data processing.**

Because of the lower SNR of Hyperion data, one may recognize fewer constituents with high-SNR in hyperspectral data. Therefore, to enhance the accuracy of the mapped minerals in the current study, the MNF-transformed images were generated for 0.4–2.4 µm and 2–2.4 µm regions. The former range presents information on the general shape of spectral profiles. The VNIR region includes absorption features of ferric iron and chlorophyll, but the SWIR region includes absorption features of $OH^-$, HOH, and $CO_3^{2-}$ [40]. Jarosite also has absorption features at 2.265 and 2.215µm in the SWIR range [41]. The number of extracted endmembers (classes) from the Hyperion scene of the Astarghan region is shown in Table 1.

**Table 1. The number of endmembers extracted by PPI from Hyperion data set of study area.**

| Wavelength range (µm) | Number of bands | Number of endmember |
|---|---|---|
| 0.4-2.4 | 139 | 4 |
| 2-2.4 | 25 | 2 |

Therefore, endmembers or target minerals were extracted from the scene using PPI method. In this case, the MNF bands were chosen and the distribution of pure pixels was investigated visually in 2-3-4- dimensional scatter plots. Generally, each cluster represents a pure endmember within the scatter plots. Then mean spectral profiles of the clusters are assumed as the target endmember spectrum. In order to recognize minerals, the spectra of the determined endmembers were compared to reference spectra provided by USGS. The similarity of the reference spectra with extracted endmembers spectra was also visually surveyed. Finally, out of the six PPI endmembers of the Hyperion scene, three endmembers were recognized. These had the highest similarity to the spectral features of kaolinite, opal, and jarosite. Figure 5 illustrates spectral profiles of identified minerals together with corresponding standard USGS spectra.

### 3.1.2. Spectral mapping

The distribution maps of the identified minerals were estimated by the matched filtering (MF) technique. Matched filters are used for recognizing a target spectrum against a background. The match filtering technique is a widely used approach in signal processing. Different matched filtering algorithms have been introduced, e.g. orthogonal subspace projection (OSP) and constrained energy minimization (CEM) [42, 43]. Equation 2 explains the MF method.

$$MF(x) = (t - m)^T S^{-1}(x - m) \quad (2)$$

Where $t$ is the target vector, $x$ is the sample vector, $m$ is the background mean and $S$ is the

background covariance [44]. In the processing of remote sensing data, the MF method serves as a suitable tool for the detection of minerals based on the degree of matching to the USGS reference spectra. MF results for identified endmembers are shown as grayscale images in Figure 6, where each pixel value demonstrates the degree to which the spectrum of reference endmembers matches the spectral profiles of identified minerals. As can be seen, the MF band of jarosite is similar to one for kaolinite. This is also observed in the field investigations that kaolinite coincided with the jarosite in the Astarghan region.

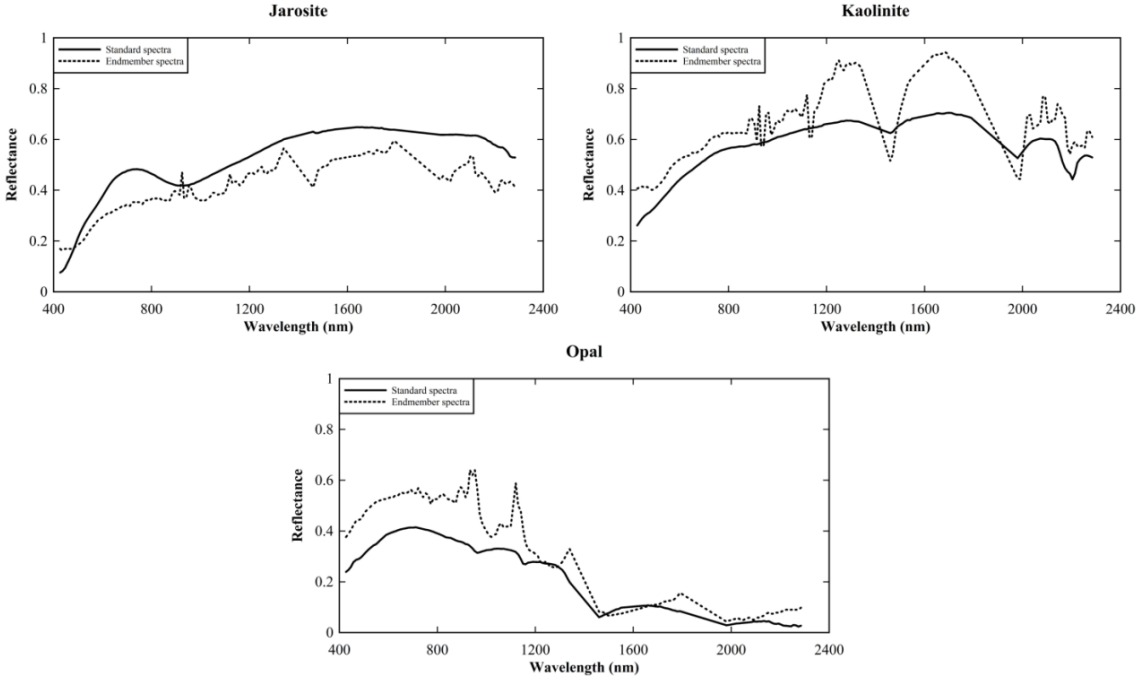


**Figure 5. The reflectance spectra of extracted endmembers from the Hyperion image of the Astarghan area together with matched USGS reference spectra. Solid line: USGS reference spectra, dashed line: spectral profiles of extracted endmembers.**

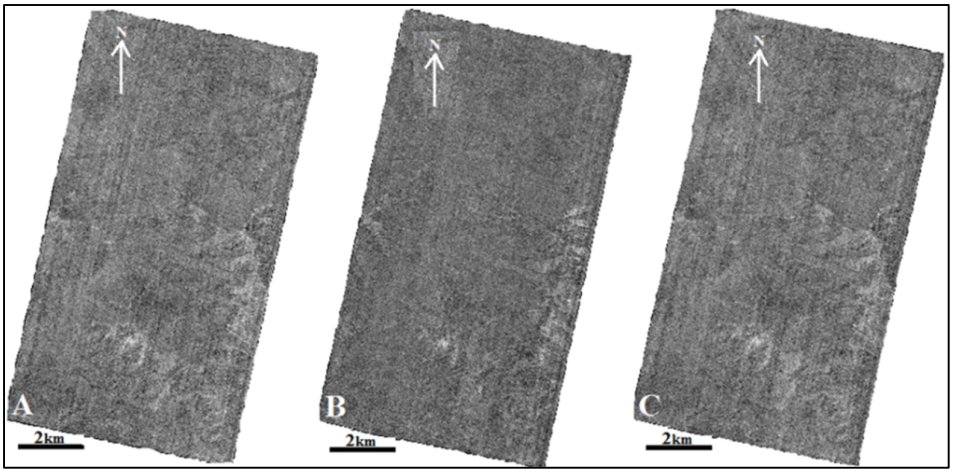


**Figure 6. MF analysis of Hyperion image of the study area: A) Kaolinite, B) Opal, C) Jarosite.**

## 4. Validation

After processing the data, the results should be validated to check their accuracy. To this end, some evaluation methods for remote sensing data are implemented [8, 45], i.e., virtual validation and validating by geological data. Virtual validation requires direct control of the remote sensing data with sufficient spatial and/or spectral resolution. In-situ verification, on the contrary, requires visiting the area of interest (i.e. field

check) and directly sampling the environment to validate the remote sensing data. Overlaying mineral distribution maps extracted from remotely sensed data with geological data is another approach for the validation of the remote sensing results. The more detailed geological data are used, the more robust validation can be performed.

In the current study, at first, the MF analysis results were verified virtually. MF technique represents the results in the form of floating-point that can be displayed as grayscale images. Virtual verification analysis reveals the constituent minerals of pixels. Therefore, if the value of pixels that contain the endmembers could be realized, then MF images can be easily classified into the background and target pixels and the distribution map of each endmember can be recognized accurately. Molan et al. [19] proposed a moving threshold for this purpose. In moving threshold, different threshold values are tested to the image histogram of each endmember, and then the threshold that leads to the maximum accuracy of the mapping of endmember is selected to classify the MF image. For example, in this study, of the various threshold values applied for opal, 0.83 was chosen to classify the corresponding MF image. That means, pixels having values higher than the threshold were assumed to contain opal, with the remaining pixels being classified as background pixels. In the case of opal, the threshold of 0.83 showed 80.64% accuracy (Figure7). In this study, 120 pixels were selected within the fraction map of the endmembers for using the moving threshold and verifying the results. The accuracy of the results was obtained by dividing the accurately mapped pixels by the total number of pixels. The total number of pixels was obtained by summing up the non-mapped pixels, accurately mapped pixels, and inaccurately mapped pixels.

Moving toward the values smaller than the threshold may increase the number of accurately and inaccurately mapped pixels, but reduces the number of non-mapped pixels. Moreover, moving toward the values larger than the threshold may reduce the number of accurately and inaccurately mapped pixels, but increases the number of non-mapped pixels. Therefore, whether to apply an upward or downward moving threshold can result in different levels of accuracy [19]. The accurately mapped pixels in the MF image describe pixels that exist in the calculated threshold of each endmember and also the fact that the existence of the endmember in the pixels is validated by virtual verification. In contrast, inaccurately mapped pixels are the ones that are in the calculated threshold of each endmember, but the existence of the endmember inside them is not validated by virtual verification. As well, non-mapped pixels correspond to pixels that are not in the calculated threshold of the endmember, but their existence is validated by the virtual verification. MF analysis using a moving threshold was performed for three endmembers, and the optimum threshold values were selected (Figure7). Comparing the MF mapping results with visual assessment of absorption features of the selected pixels spectra, an agreement of 78.06% was obtained (Table 2).

**Table 2. Accuracy values of mapped endmembers by MF method evaluated by virtual verification.**

| | endmembers | | | Total |
|---|---|---|---|---|
| | Kaolinite | Opal | Jarosite | |
| Accurate mapped pixels | 70 | 75 | 65 | 210 |
| Inaccurate mapped pixels | 4 | 5 | 6 | 15 |
| Not mapped pixels | 15 | 13 | 16 | 44 |
| Accuracy (%) | 78.65 | 80.64 | 74.71 | 78.06 |

Notice that in Table 3, the total number of pixels for each endmember is lower than 120. This is because the selected pixels that pertained to the background were ignored in the accuracy calculation (i.e. the pixels with values below the threshold and those with spectra dissimilar to the endmember were disregarded). In this study, the threshold value with the highest accuracy was introduced as the optimum threshold value for each mineral.

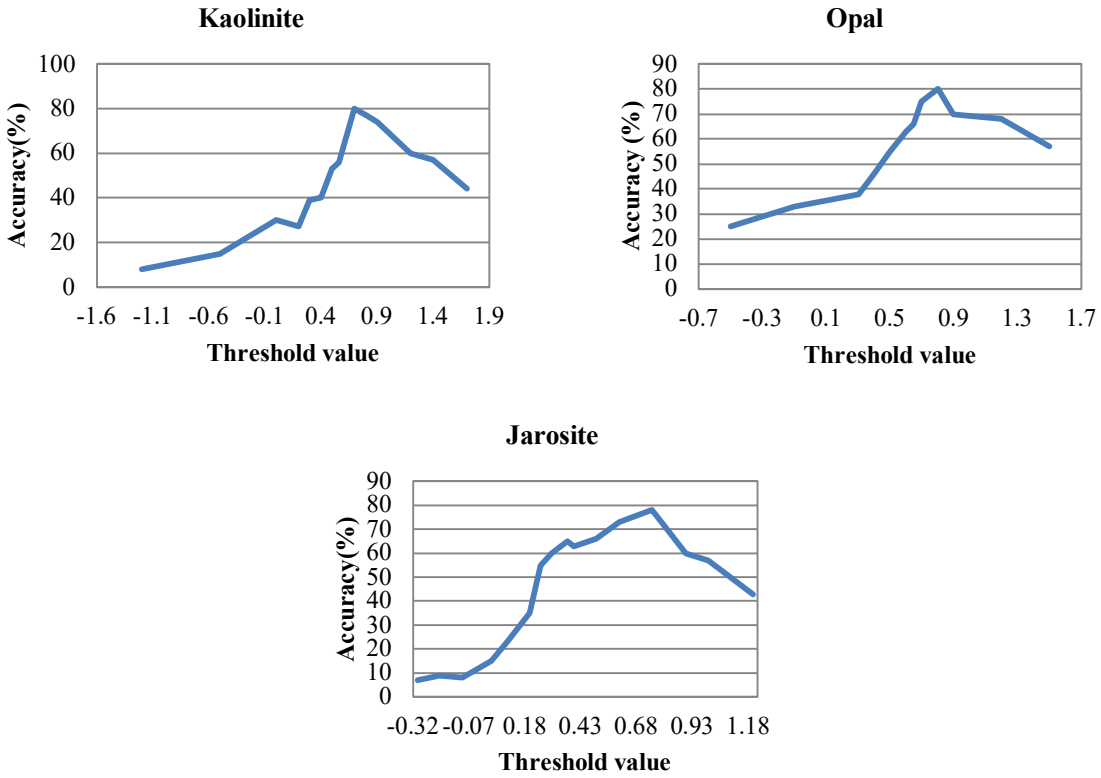


**Figure7. Accuracy analysis of various applied threshold values corresponds to MF images of endmembers.**

Another validation was made using the 1:20000 geological map of the study area. In the current approach, the feasible lithologies which can comprise a mineral were selected for each extracted endmember using the union function of the ArcGIS v. 10.2 software. Then, for each endmember, the "Intersect" overlay function was implemented for delineating the intersection of its abundant areas (derived from the moving threshold technique on MF analysis) with feasible lithologies. The feasible lithologies corresponding to each endmember according to the field investigations are tabulated in Table 3. The ratio of the area of intersection to the total distribution area can be used as a metric for evaluating the accuracy of the mineral mapping approach. The ratio of one indicates that the extracted distribution areas by using of moving threshold method for an endmember are whole inside the lithological units that can comprise it. According to the results of the overlay functions, 62% of jarosite are distributed in 35% of the study area. In this case, 35% of the study area is covered by jarosite-bearing lithologies. The one for opal is 63% in 41%, and for kaolinite is 77% in 41%. The overlay maps are indicated in Figure 8.

Three chip samples were selected from lithological units including opal, kaolinite, and jarosite. Then, the samples were analyzed by the XRD method. XRD analysis is an effective method for identifying the mineral phases. Table 4 shows the results of the XRD analysis of samples that are consistent with the lithological units. In addition, the spectra obtained from XRD analysis are also shown in Fig 9. Finally, applying the optimum threshold values, the distribution map of alteration minerals in the Astarghan area along with the location of sampling from the area's indicative alterations is shown in Figure 10.

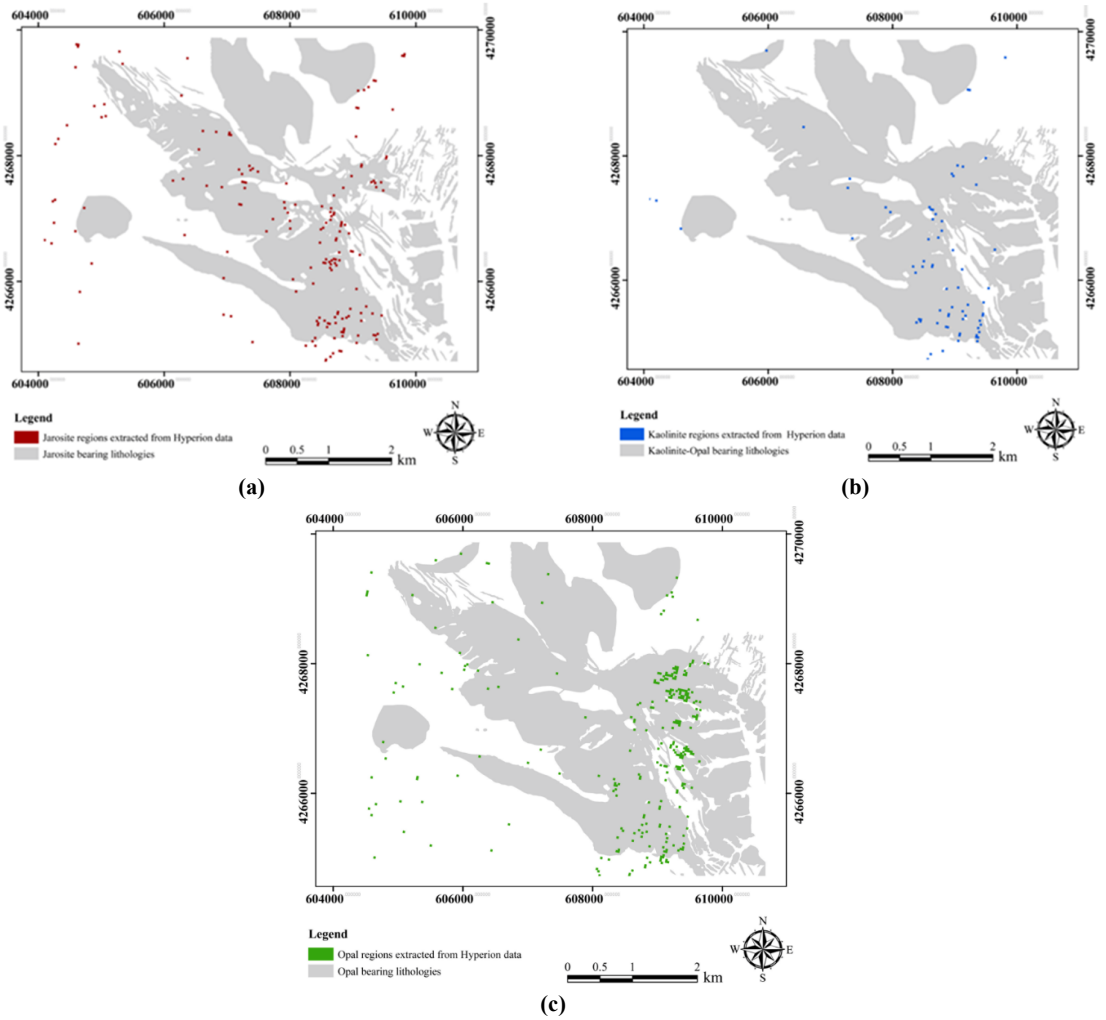


**Figure 8. Overlay map of the minerals distribution areas extracted by moving threshold technique and a) jarosite, b) kaolinite, c) opal bearing lithological units.**

**Table 3. The list of lithologies that can comprise endmembers according to the field investigations.**

| Endmember | Feasible lithologies list |
|---|---|
| Jarosite | Porphyry diorite, micro-diorite to quartz-monzodiorite, porphyritic to granular granite-granodiorite, sill, dike swarm, vein veinlets, andesite, skarn, elluvium. |
| Kaolinite | Porphyry diorite, micro-diorite to quartz-monzodiorite, porphyritic to granular granite-granodiorite, sill, dike swarm, vein veinlets, hornfels, andesite, Contact metamorphic rocks, terrace, skarn, elluvium. |
| Opal | Porphyry diorite, micro-diorite to quartz-monzodiorite, porphyritic to granular granite-granodiorite, sill, dike swarm, vein veinlets, hornfels, andesite, Contact metamorphic rocks, terrace, skarn, elluvium. |

**Table 4. Minerals identified using XRD for three samples.**

| No.sample | Major phase(s) | Minor phase(s) |
|---|---|---|
| 1 | Kaolinite (Al2Si2O5(OH)4) | Goethite (FeO(OH)) |
| 2 | Quartz (SiO2), Kaolinite (Al2Si2O5(OH)4) | Clay mineral(IIIite or/& Smectite group) |
| 3 | Jarosite (KFe3(So4)2.(OH)6) | Scorodite (FeAsO4,2H2O), Quartz (SiO2) |

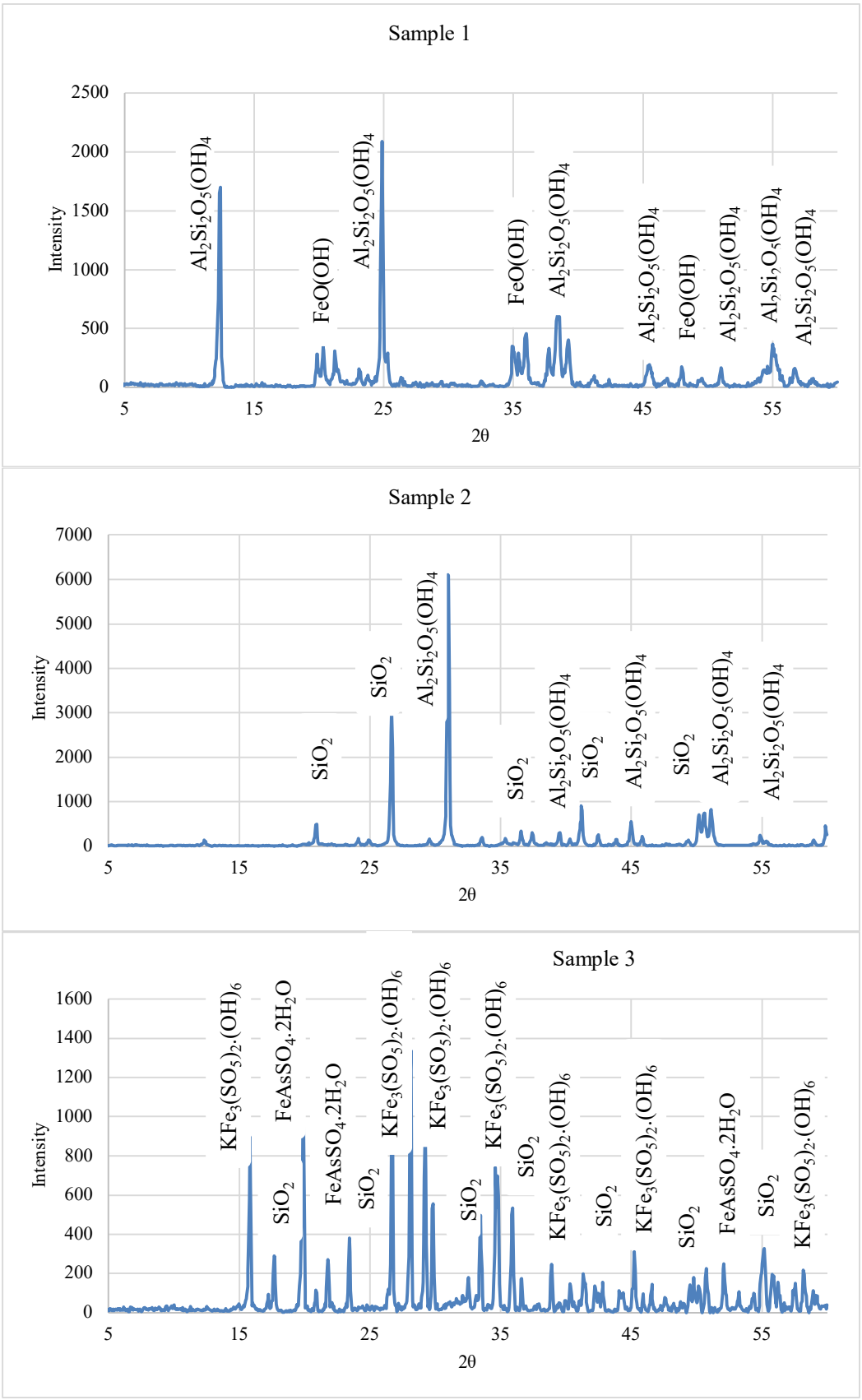


**Figure 9. The spectra obtained from XRD analysis for lithological units.**

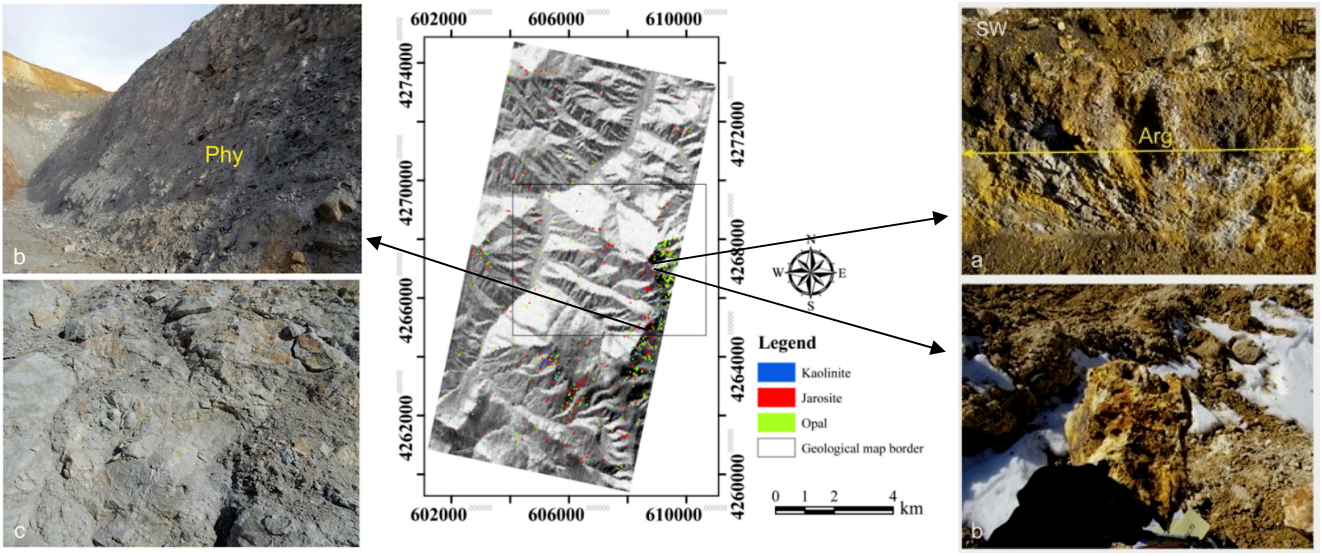


**Figure 10. Distribution map of alteration minerals in the Astarghan area that extracted by implementing the moving threshold technique on MF bands along with the location of samples from the area of indicative alterations (two right-hand pictures, i.e., a and b, are related to the argellic alteration zones that show the location of XRD samples, i.e., S1&S2, also two left-hand pictures, i.e., c and d, are related to the phyllic zones that show the location of XRD sample, i.e., S3).**

## 5. Discussion

In general, one of the most important problems in image processing, especially hyperspectral data, is the presence of noise in the data. With the increase of noise in the data, processing is more difficult and it is necessary to use more accurate methods to extract information. However, the use of noise reduction and denoising methods such as SNR and MNF can relatively solve this shortcoming, but the presence of noise in some data with high noise is still noticeable.

Hyperion data as hyperspectral space-born data has these conditions. Therefore, different methods should be used to process this type of data and validate the resulting maps properly. In this study, the most common processing method for hyperspectral data, i.e., the unmixing method was used. Noticeably, by investigating both linear and nonlinear unmixing methods it concluded that due to the noise intensity of Hyperion images the use of nonlinear unmixing methods has no effects on the quality of the results. Therefore, a linear unmixing method, i.e., AIG was applied. Moreover, in this research, in addition to applying the PPI method on all MNF bands, in order to get more reliable results, Hyperion bands in the SWIR range were also separately analyzed because the SWIR is a suitable wavelength range for investigating mineral spectral features. Therefore, as seen in Table 1, two endmembers were extracted by analyzing 25 bands in the spectral range of 2 µm to 2.4 µm, in which there is a good agreement between the spectral of these endmembers and the spectral of jarosite and kaolinite minerals.

After identifying the endmembers, i.e., three members, the abundance of each member in the image by the match filtering method was determined. Due to the intensity of noise in Hyperion data, accurate mapping of the minerals abundance is a challenging task. So, to cope with this challenge Moving Threshold method was applied. The main advantage of the Moving Threshold method is measuring the accuracy of different thresholds and giving the best abundance map for each endmember. In other words, Moving Threshold, through statistical analysis of image pixels, helps the user to find a more accurate abundance map.

To validate the performance of the Moving Threshold method, a comparison was made between the final abundance map of each endmember with the detailed geological map of Astarghan area, in which results show an acceptable agreement between them. As well, taken samples from the identified areas also showed a good coincidence between the major detected phase of XRD and the detected end members in the study area.

## 6. Conclusions

In general, the application of effective processing techniques for hyperspectral data

analysis is the key step for alteration zones mapping. In this study, the distribution of alteration minerals in the Astarghan area (NW-Iran) was successfully mapped by using Hyperion data analysis. For this purpose, at first, the MNF transformation was performed. Then pure endmembers were extracted using PPI computation and n-d visualizer. The MF approach was used to analyze the Hyperion data to map the distribution of the endmembers. The separation of MF grayscale into background and target pixels is a challenge in the MF analysis. To address this issue in the present study, the concept of moving threshold was introduced into the MF analysis of Hyperion imagery. Moving threshold is a useful technique to find proper values in order to separate MF images into the target and background pixels. The results of the MF analysis were statistically validated by the virtual verification method by comparing the spectrums of three extracted minerals to the USGS spectral library. The conformity between the MF results and virtual verification was about 78%. The results were further verified using the geological settings (1:20000 geological map of the Astarghan area). Overlaying the extracted minerals distribution maps with digitized maps of the lithological units in ArcGIS software shows a good consistency between them so that the majority of distribution areas of minerals coincide with proper geological units. The field studies indicated argillic, phyllic, and propylitic alteration zones across the Astarghan region. Moreover, field studies demonstrated that the most extensive alteration zone in the study area was argillic, which itself consisted of quartz, kaolinite, illite, and dickite. Furthermore, across the central part of the study area, there was a supergene advance argillic alteration that consists of jarosite, quartz, and clay minerals, and these minerals were defined as the representatives of the argillic zone. Based on the final map of alteration minerals obtained from the analysis of Hyperion data by moving threshold method and the field investigations, there is a high consistency between the results of this study and field observations such that the pixels of alteration minerals in the final map (figure 10) correspond to the areas of alterations that occurred in the Astarghan region. As well, three samples from extracted mineral distribution areas (MFs) were also selected and their XRD analysis results were in good agreement with our outputs. As future research, the moving threshold method can be performed on more recent hyperspectral data such as PRISMA and check the accuracy of the results.

## References

[1]. Poormirzaee, R. & Oskouei, M.M. (2010). Use of spectral analysis for detection of alterations in ETM data, Yazd, Iran. *Appl Geomat, 2*, 147–154.

[2]. Saed, S, Azizi, H., Daneshvar, N., Afzal, P., Whattam, S.A. & Mohammad, Y.O. (2022). Hydrothermal alteration mapping using ASTER data, Takab-Baneh area, NW Iran: A key for further exploration of polymetal deposits. *Geocarto International, 37(26)*, 11456-11482.

[3]. Pourgholam, M. M., Afzal, P., Adib, A., Rahbar, K., & Gholinejad, M. (2022). Delineation of Iron alteration zones using spectrum-area fractal model and TOPSIS decision-making method in Tarom Metallogenic Zone, NW Iran. *Journal of Mining and Environment*, *13(2)*, 503-525.

[4]. Gersman, R., Ben-Dor, E., Beyth, M., Avigad, D., Abraha, M. & Kibreba, A. (2008). Mapping Of hydrothermally altered rocks by the EO-1 Hyperrion sensor, northern Danakil, Eritrea. *Int. J. Remote Sens., 29(13)*, 3911–3936.

[5]. Goetz, A.F.H. (2009). Three decades of hyperspectral remote sensing of the Earth: A personal view. *Remote Sensing of Environment*, *113 (1)*.

[6]. Kruse, F.A. (2003). Mineral mapping with AVIRIS and EO-1 Hyperion. Presented at the 12th JPL Airborne Geoscience Workshop, Pasadena, California.

[7]. SrinivasaPerumal, P., Shanmugam, S. & Ganapathi, P. (2020). Satellite imagery and spectral matching for improved estimation of calcium carbonate and iron oxide abundance in mine areas. *Arabian Journal of Geosciences*, *13(18)*, 1-13.

[8]. Oskouei, M.M. & Babakan, S. (2016). Detection of alteration minerals using Hyperion data analysis in Lahroud. *Journal of the Indian society of remote sensing*, *44(5)*, 713-721.

[9]. Cudahy, T.J., Hewson, R., Huntington, J.F., Quigley, M.A. & Barry, P.S. (2001). The performance of the satellite-borne Hyperion hyperspectral VNIR-SWIR imaging system for mineral mapping at Mount Fitton, South Aust. IEEE IGARSS proc. pp: 9–13.

[10]. Pour, B.A., Hashim, M. & Marghany, M. (2011). Using spectral mapping techniques on short wave infrared bands of ASTER remote sensing data for alteration mineral mapping in SE Iran. *Int J Physical Sci.*, *6(4)*, 917–929.

[11]. Ekanayake, E. M. M. B., Vithana, S. S. P., Ekanayake, E. M. H. E. B., Rathnayake, A. R. M. A. N., Abeysekara, A. M. R., Oorloff, T. S. J., ... & Senaratne, A. (2019). Mapping ilmenite deposit in Pulmudai, Sri Lanka using a hyperspectral imaging-based surface mineral mapping method. *Journal of the National Science Foundation of Sri Lanka, 47(3)*, 271-284.

[12]. Vignesh, K. & Kiran, Y. (2020). Comparative analysis of mineral mapping for hyperspectral and multispectral imagery. *Arabian Journal of Geosciences*, *13(4)*, 1-12.

[13]. Bi, X., Miao, F. & Ye, C. (2012). Lithology identification and mapping by hyperion hyperspectral remote sensing. *Comput Tech Geophys Geochem Explor*, *34*, 599-603.

[14]. Wang, J., Zhou, G., Zhang, Y., Bussink, C., Zhang, J. & Ge, H. (2016). An unsupervised mixture-tuned matched filtering-based method for the remote sensing of opium poppy fields using EO-1 Hyperion data: An example from Helmand, Afghanistan. *Remote Sensing Letters, 7(10)*, 945-954.

[15]. Govil, H., Gill, N., Rajendran, S., Santosh, M. & Kumar, S. (2018). Identification of new base metal mineralization in Kumaon Himalaya, India, using hyperspectral remote sensing and hydrothermal alteration. *Ore Geology Reviews*, *92*, 271-283.

[16]. Khatun, M., Sharma, R.U. & Chattoraj, S.L. (2019). Mineralogical mapping using field and image based spectra in parts of Delhi-Aravalli Fold Belt, Rajasthan, India. *International Journal of Economic and Environmental Geology*, 8-14.

[17]. Pan, Z., Liu, J., Ma, L., Chen, F., Zhu, G., Qin, F. & Wang, J. (2019). Research on hyperspectral identification of altered minerals in Yemaquan West Gold Field, Xinjiang. *Sustainability, 11(2)*, 428.

[18]. Boardman, J.W. (1998). Leveraging the high dimensionality of AVIRIS data for improved sub-pixel target unmixing and rejection of false positives: mixture tuned matched filtering. In: Summaries of the Seventh Annual JPL Airborne Geoscience Workshop, Pasadena, CA, pp. 55.

[19]. Molan, Y.E., Refahi, D. & Tarashti, A.H. (2014). Mineral mapping in the Maherabad area, eastern Iran, using the HyMap remote sensing data. *International Journal of Applied Earth Observation and Geoinformation*, *27*, 117–127.

[20]. Ferdowsi, R., Calagari, A.A., Houseinzadeh, M.R. & Seyahcheshm, K. (2016). Studies of alteration zones of Astarghan area based on spectral behaviour of alteration minerals, mineralogy and Fluid Inclusions signatures, Kharvana, East- Azarbidjan. 34th national geosciences symposium, Tehran, Iran.

[21]. Ferdowsi, R., Calagari, A.A., Simmonds, V. & Miranvari, A. (2021). Evolution of the gold (copper) mineralization in the porphyry stock and the related skarn zones and epithermal veins in the Astarghan area, NW Iran: Evidence from fluid inclusion, mineral chemistry and sulfur isotope analyses. *Ore Geology Reviews, 136*, 104196.

[22]. Mehrpartov, M. (1997). 1:100000 Geological Map and geological report of Siahrood. Geological survey of Iran (GSI).

[23]. Hosseinjanizadeh, M., Tangestani, M.H., Roldan, F.V. & Yusta, I. (2014). Sub-pixel mineral mapping of a porphyry copper belt using EO-1 Hyperion data. *Advances in Space Research, 53 (3)*, 440-451.

[24]. Barry, P.S. (2001). [EO-1/ Hyperion Science Data User's Guide, Level 1_B], TRW Space, Defense & Information Systems, Redondo Beach, CA.

[25].Bindschadler, R. & Choi, H. (2003). Characterizing and correcting Hyperion detectors using ice-sheet images. *IEEE Transactions on Geoscience and Remote Sensing*, *41(6)*, 1189-1193.

[26]. Scheffler, D. & Karrasch, P. (2013). Preprocessing of Hyperspectral Images-a Comparative Study of Destriping Algorithms for EO-1 Hyperion. Image and Signal Processing for Remote Sensing, edited by Lorenzo Bruzzone, Proc. of SPIE Vol. 8892, 88920.

[27]. Pande-Chhetri, R. & Abd-Elrahman, A. (2012). Filtering high-resolution hyperspectral imagery in a maximum noise fraction transform domain using wavelet-based de-striping. *Int. J. of Remote Sensing 34(6)*, 2216-2235.

[28]. RSI, 2000. ENVI User's Guide, the Environment for Visualizing Images, Version 3.2. Research Systems, 2995 Wilderness Place, Boulder, CO 80301, USA.

[29]. Oskouei, M.M. & Babakan, S. (2016). Role of smile correction in mineral detection on hyperion data. *Journal of Mining & Environment*, *7(2)*, 261-272.

[30]. Goodenough, D.G., Dyk, A., Niemann, K.O., Pearlman, J.S., Hao, C., Tian, H., Murdoch, M. & West, C. (2003). Processing Hyperion and Ali for forest classification. *IEEE Transactions on Geoscience and Remote Sensing, 41 (6)*, 1321-1331.

[31]. Fuyi, T., Mohammed, S., Abdullah, K., Lim, H. & Ishola, K., (2013). A comparison of atmospheric correction techniques for environmental applications. IEEE International Conference on Space Science and Communication (IconSpace).

[32]. Poormirzaee, R., & Mohammadi Moskouei, M. (2012). Topographic correction of hyperspectral data of west east-Azarbayjan. *Journal of Mining Engineering*, *7(15)*, 25-33.

[33]. Riaño, D., Chuvieco, E., Salas, J. & Aguado, I. (2003). Assessment of different topographic corrections in Landsat-TM data for mapping vegetation types. *IEEE Transactions on Geoscience and Remote sensing, 41(5)*, 1056-1061.

[34]. Khurshid, K.S., Staenz, K., Sun, L., Neville, R., White, H.P., Bannari, A., Champagne, C.M. & Hitchcock, R. (2006). Preprocessing of EO-1 Hyperion Data. *Canadian Journal of Remote Sensing*, *32(2)*, 84–97.

[35]. Keshbava, N. & Mustard, J.F., (2002). Spectral unmixing. IEEE signal processing magazine. 1053-5888/02/S17.00.

[36]. Bioucas-Dias, J.M., Plaza, A., Dobigeon, N., Parente, M., Du, Q., Gader, P. & Chanussot, J. (2012). Hyperspectral Unmixing Overview: Geometrical, Statistical, and Sparse Regression-Based Approaches. *IEEE Journal of Selected Topics in Applied Earth Observations and Remote Sensing, 5(2)*, 354-379.

[37]. Dobigeon, N., Altmann, Y., Brun, N. & Moussaoui, S. (2016). Linear and nonlinear unmixing in hyperspectral imaging. *Data Handling in Science and Technology: Resolving Spectral Mixtures*, 41.

[38]. Boardman, J.W. (1993). Automated spectral unmixing of AVIRIS data using convex geometry concepts. In Summaries, Fourth JPL Airborne Geoscience Workshop, JPL Publication, 93-26, 1, p. 11-14.

[39].Chang C-I. 2013. Hyperspectral data processing: algorithm design and analysis. John Wiley & Sons.

[40]. Green, A.A., Berman, M., Switzer, B. & Craig, M.D. (1988). A transformation for ordering multispectral data in terms of image quality with implications for noise removal. *IEEE Transactions on Geoscience and Remote Sensing, 26(1)*, 65 - 74.

[41]. Clark, R.N. (1999). Spectroscopy of rocks and minerals, and principles of spectroscopy. In: Rencz, A.N. (Ed.), Manual of Remote Sensing. Remote Sensing for the Earth Sciences. John Wiley & Sons, New York, pp. 3–58.

[42]. Harsanyi, J.C., Farrand, W.H. & Chang, C.I. (1994). Detection of subpixel signatures in hyperspectral image sequences. Proceedings of 1994 ASPRS Annual Conference, Reno, Nevada, pp 236–247.

[43]. Chang, C-I. (2005). Orthogonal subspace projection (OSP) revisited: A comprehensive study and analysis. *IEEE transactions on geoscience and remote sensing, 43(3)*,502-518.

[44]. Schott, J.R. (2007). Remote Sensing, The Image Chain Approach, second ed. Oxford University Press, New York, pp. 688.

# استفاده از تصاویر فراطیفی هایپریون در به نقشه درآوردن کانی‌های مرتبط با دگرسانی در منطقه آسترقان واقع در شمالغرب ایران

**راشد پورمیرزائی[1*] و هادی جمشید مقدم[2]**

**۱- گروه مهندسی معدن، دانشگاه صنعتی ارومیه، ارومیه، ایران**
**۲- دانشکده مهندسی معدن، دانشگاه صنعتی سهند تبریز، تبریز، ایران**

ارسال ۲۰۲۴/۰۵/۰۹، پذیرش ۲۰۲۴/۰۶/۲۸

* نویسنده مسئول مکاتبات: rashed.poormirzaee@gmail.com

**چکیده:**

در سال‌های اخیر، داده‌های فراطیفی به طور گسترده در علوم زمین مورد استفاده قرار گرفته‌اند، چراکه این داده ها اطلاعات طیفی دقیقی از سطح زمین ارائه می دهند. هدف این تحقیق استفاده از روش فیلتر تطبیقی (MF) بر روی تصاویر فراطیفی هایپریون برای به نقشه درآوردن کانی‌های دگرسانی در منطقه آسترقان است. آسترقان در شمال غربی ایران قرار دارد که در آن کانسار طلای اپی ترمال کم سولفید به شکل استوک ورک و رگه‌ای گزارش شده است. در این مطالعه ابتدا بر روی تصاویر هایپریون آسترقان تصحیح توپوگرافی و اتمسفری انجام گرفت. سپس کیفیت داده‌ها برای شناسایی و حذف باندهای بد، جهت بهبود دقت مراحل پردازش بعدی بررسی شد. اما در روش MF، تفکیک تصویر مربوطه به پیکسل‌های هدف و پس زمینه یک چالش است. در این مقاله برای رفع این چالش، یک تکنیک آماری (آستانه متحرک) پیشنهاد شده است. بعد از اعمال این روش بر روی تصاویر مورد مطالعه نتایج بیانگر فراوانی سه کانی شاخص: کائولینیت، اوپال و ژاروسیت در منطقه بود. جهت ارزیابی نتایج از دور روش ارزیابی مجازی (استفاده از کتابخانه طیفی) و همچنین استفاده از بررسی‌های صحرایی استفاده شد. ارزیابی نتایج با استفاده از داده‌های کتابخانه طیفی سازمان زمین‌شناسی ایالات متحده (USGS) صحت ۷۸/۰۶٪ را نشان داد. علاوه بر این، مقایسه نتایج با بررسی‌های صحرایی و اطلاعات زمین شناسی موجود بیانگر عملکرد بسیار مناسب روش پیشنهادی در این مطالعه در به نقشه‌درآوردن کانی‌های دگرسانی بود. جهت ارزیابی ترکیب کانی‌های شناسائی شده بر روی تصاویر هایپریون، از نتیجه آنالیز XRD سه نمونه سنگ استفاده شد.

**واژه‌های کلیدی:** داده‌های هایپریون؛ فیلتر تطبیق؛ آستانه متحرک؛ به نقشه درآورن کانی‌ها.